JGR Solid Earth

RESEARCH ARTICLE
10.1029/2018JB016470

The Impact of Noise in a GRACE/GOCE Global Gravity Model on a Local Quasi-Geoid

Cornelis Slobbe[1], Roland Klees[1], Hassan H. Farahani[2], Lennard Huisman[3], Bas Alberts[4], Pierre Voet[5], and Filip De Doncker[5]

[1]Delft University of Technology, Delft, The Netherlands, [2]Geodätisches Institut, Stuttgart, Germany, [3]Kadaster, Apeldoorn, The Netherlands, [4]Rijkswaterstaat Centrale Informatievoorziening, Delft, The Netherlands, [5]Nationaal Geografisch Instituut, Brussel, Belgium

Key Points:
- For the first time ever, we used a satellite-only GGM with full noise variance-covariance matrix as data set in local quasi-geoid modeling
- For our area of interest, the impact of the noisy GGM on the local quasi-geoid model has a peak-to-peak amplitude of 7.8 cm
- The impact of using a simplified noise model of the GGM is significant, in particular if variance component estimation is used

Correspondence to:
C. Slobbe,
d.c.slobbe@tudelft.nl

Citation:
Slobbe, C., Klees, R., Farahani, H. H., Huisman, L., Alberts, B., Voet, P., & Doncker, F. D. (2019). The impact of noise in a GRACE/GOCE global gravity model on a local quasi-geoid. *Journal of Geophysical Research: Solid Earth*, *124*, 3219–3237. https://doi.org/10.1029/2018JB016470

Received 27 JUL 2018
Accepted 2 MAR 2019
Accepted article online 7 MAR 2019
Published online 30 MAR 2019

Abstract We present a local quasi-geoid (QG) model which combines a satellite-only global gravity model with local data sets using weighted least squares. The QG is computed for an area comprising the Netherlands, Belgium, and the southern North Sea. It uses a two-scale spherical radial basis function model complemented by bias parameters to account for systematic errors in the local gravity data sets. Variance factors are estimated for the noise covariance matrices of all involved data sets using variance component estimation. The standard deviation (SD) of the differences between the computed QG and GPS/leveling data is 0.95 and 1.52 cm for the Netherlands and Belgium, respectively. The fact that the SD of the control data is about 0.60 and 1.20 cm for the Netherlands and Belgium, respectively, points to a lower mean SD of the computed QG model of about 0.7 cm for the Netherlands and 1.0 cm for Belgium. The differences to a QG model computed with the remove-compute-restore technique range from −5.2 to 2.6 cm over the whole model domain and from −1.5 to 1.5 cm over the Netherlands and Belgium. A variogram analysis of the differences with respect to GPS/leveling data reveals a better performance of the computed QG model compared to a remove-compute-restore-based QG model for wavelengths >100 km for Belgium but not for the Netherlands. The latter is due to the fact that at the spatial scales resolved by the global gravity model, variance component estimation assigns significantly lower weights to the local data set in favor of the global gravity model.

1. Introduction

More than 10 years after the launch of, respectively, the Gravity Recovery and Climate Experiment (GRACE) and the Gravity field and steady-state Ocean Circulation Explorer (GOCE) satellite gravimetry missions, one might expect that the acquired data are routinely combined with other data sets in a *statistically optimal way* to estimate local quasi-geoid (QG) models. This will improve the quality of the estimated QG model for most areas in the world.

The reality is, however, different. The standard approach to local QG modeling is still the remove-compute-restore (RCR) technique (Sjöberg, 2005a, and cited studies). The main concern with the RCR technique is that it does not use the global gravity model (GGM) in the same way as the local data sets; in fact, when using the RCR technique, the main role of the GGM is to facilitate a local approach to QG modeling. This may lead to a suboptimal QG model, in particular at those wavelengths where the quality of the GGM is superior or comparable to the one of the local data sets. Though a number of data combination approaches have been suggested to address this concern (e.g., Chambodut et al., 2005; Denker, 2013; Lieb et al., 2016; Schuh et al., 2015; Sjöberg, 2011; Wu et al., 2017), no studies based on real data sets are known yet, which make fully use of the latest generation of satellite-only GGMs and use realistic noise models for all involved data sets.

In this study, we combine a GGM-based data set with local data sets and estimate a local QG model using weighted least squares techniques. The computed QG model will be used to answer two main questions:

1. *What is the impact of a noisy GGM on a local QG model?* This question will be answered by comparing the QG model with a QG model computed with the RCR technique. The RCR-based QG model used in this study is significantly better than the model in Wu et al. (2017). Some of the data sets used in Wu et al. (2017) suffer from systematic errors, which were not corrected for. Moreover, the GPS/leveling control data set

over Belgium used in Wu et al. (2017) is a preliminary data set, which comprises a subset of the control data set used in our study, and suffers from systematic errors on the order of several centimeters, which were not known at the time the study (Wu et al., 2017) was conducted.

2. *Does the weighted least squares combination of a GGM with local data sets improve the quality of the QG model?* This question will be answered by comparing the two QG models mentioned before with independent GPS/leveling data. Moreover, we compared the combined QG model with the European Gravimetric (Quasi)-Geoid EGG2015 (Denker, 2015), which combines a GGM with local data sets using the spectral combination technique of Wenzel, (1982; cf. Denker, 2013 for a review about the spectral combination technique).

The two main questions are complemented by two additional questions:

3. *What is the impact on the computed QG model when the coarse spatial scales of the local QG model are only determined by the GGM?* As far as the contribution of a GGM to a local QG model is concerned, this solution is the opposite to a solution obtained with the RCR technique. Comparing this solution with a RCR-based solution provides an upper bound on the potential contribution of a GGM and indicates whether the combination of a GGM with local data sets has any added value.
4. *What is the impact on the computed QG model of using a simplified noise model for the GGM-based data set?* Here two alternative scenarios will be considered. The first is motivated by the fact that the most advanced QG models currently available, which combine a GGM with local data sets, only use information about the noise variances but ignore the noise covariances. The second addresses the fact that many methods and software packages currently in use cannot deal with full, highly ill-conditioned noise VC matrices. For instance, Klees et al. (2018) have shown that the noise covariance matrix of the GOCO05s GGM, which represents the state of the art of satellite-only GGMs and is used here, is highly ill conditioned making the computation of the weight matrix unstable.

The remainder of the paper is organized as follows. In section 2, we present the methodology used to conduct the statistically optimal combination of the local data sets and the GGM. In section 3, we describe the data sets used in the numerical study including the data preprocessing. Section 4 outlines the setup of the numerical experiments conducted to answer the research questions. In section 5, we present and discuss the results. Finally, we conclude by emphasizing the main findings.

2. Methodology of Data Combination

We use the approach of Klees et al. (2017) to combine a noisy GGM with noisy local data sets using weighted least squares techniques. Here the key elements of this approach are outlined for convenience using a more compact notation. After residual terrain modeling (RTM), the disturbing potential T is assumed to be band limited to a maximum degree L_{T}. It is parameterized using a two-scale spherical radial basis function (SRBF) model

$$T(x) = \sum_{q=1}^{Q_0} d_{q,0}\Psi_{q,0}(x, z_{q,0}) + \sum_{q=1}^{Q_1} d_{q,1}\Psi_{q,1}(x, z_{q,1}). \tag{1}$$

Here Q_0 and Q_1 are the number of SRBFs used to model the coarse and detail spaces, respectively, the sets $\{d_{q,0}\}$ and $\{d_{q,1}\}$ comprise the scale-dependent model parameters to be estimated, and the sets $\{\Psi_{q,0}\}$ and $\{\Psi_{q,1}\}$ comprise the SRBFs, which are defined as

$$\Psi_{q,0}(x, z_{q,0}) = \frac{R}{|x|}\sum_{l=0}^{L_{\mathrm{GGM}}} \phi_l h_l \left(\frac{|z_{q,0}|}{|x|}\right)^l Q_l(\hat{x}\cdot\hat{z}_{q,0}), x \in \overline{\mathrm{ext}\sigma_R}, z_{q,0} \in \mathrm{int}\sigma_R, \tag{2}$$

$$\Psi_{q,1}(x, z_{q,1}) = \frac{R}{|x|}\sum_{l=0}^{L_{\mathrm{T}}} \phi_l (1-h_l) \left(\frac{|z_{q,1}|}{|x|}\right)^l Q_l(\hat{x}\cdot\hat{z}_{q,1}), x \in \overline{\mathrm{ext}\sigma_R}, z_{q,1} \in \mathrm{int}\sigma_R. \tag{3}$$

$z_{q,0}$ and $z_{q,1}$ are the centers of the SRBFs $\Psi_{q,0}$ and $\Psi_{q,1}$, respectively, Q_l is the reproducing kernel of the space of harmonic functions of degree l, ϕ_l is the Legendre coefficient of degree l, $\hat{x} = \frac{x}{|x|}$ and $\hat{z} = \frac{z}{|z|}$ are points on the unit sphere, σ_R is the surface of a sphere of radius R, L_{GGM} is the maximum spherical harmonic degree of the GGM, and L_{T} is the maximum spherical harmonic degree that the local data sets allow to resolve.

For points x outside the Earth masses, equation (1) is used as the model of the disturbing potential. The first term of equation (1) represents the spatial scales, which are resolved by the GGM. In that sense, it represents the coarse scales of the disturbing potential. The second term of equation (1) adds the details up to the smallest scale that are resolved by the local data sets. Hence, the set of basis functions $\{\Psi_{q,1}(x, z_{q,1})\}$ spans a detail space, which complements the coarse-scale space spanned by the set of basis function $\{\Psi_{q,0}(x, z_{q,0})\}$. The filter coefficients h_l are chosen as

$$h_l = \begin{cases} 1, & l < p_1 \\ 0.5 + 0.5\cos\left(\pi \frac{l-p_1}{p_2-p_1}\right), & p_1 \le l \le p_2 \le L_{\mathrm{GGM}} \\ 0, & l > p_2 \end{cases}. \tag{4}$$

Equation (4) defines a cosine taper, which acts as a low-pass filter. The characteristics of the low-pass filter are fully described by the two parameters p_1 and p_2.

Klees et al. (2017) have shown that a simultaneous estimation of the model parameters $\{d_{q,0}\}$ and $\{d_{q,1}\}$ from all data sets suffers from signal leakage, that is, high-frequency signal in the local data sets leaks into $\{d_{q,0}\}$ and low-frequency signal in all data sets leaks into $\{d_{q,1}\}$. To minimize signal leakage, they recommend to estimate the model parameters sequentially:

Step 1: Weighted least squares estimation of the model parameter set $\{d_{q,1}\}$ of equation (1) from the local data sets using the classical RCR technique. The model parameters $\{d_{q,1}\}$ of equation (1) are (also) the parameters of a single-scale model of the disturbing potential, which is

$$T = \sum_{q=1}^{Q_1} d_{q,1}\Phi_{q,1}(x, z_{q,1}). \tag{5}$$

The basis functions $\{\Phi_{q,1}\}$ span the whole space up to the smallest scale that is resolved by the local data sets. They are defined as

$$\Phi_{q,1}(x, z_{q,1}) = \frac{R}{|x|}\sum_{l=0}^{L_T}\phi_l\left(\frac{|z_{q,1}|}{|x|}\right)^l Q_l(\hat{x}\cdot\hat{z}_{q,1}),\ x \in \overline{\mathrm{ext}\,\sigma_R},\ z_{q,1} \in \mathrm{int}\ \sigma_R. \tag{6}$$

Note that the model parameters $\{d_{q,1}\}$ in equation (5) are the same as in equation (1). The base functions in both equations are, however, different (cf. equations (3) and (6)).

Step 2: Weighted least squares estimation of the model parameters $\{d_{q,0}\}$ of equation (1) using the coarse-scale model

$$T_{\mathrm{cs}} = \sum_{q=1}^{Q_0} d_{q,0}\Psi_{q,0}(x, z_{q,0}). \tag{7}$$

The model parameters $\{d_{q,0}\}$ are estimated using two data sets: (i) height anomalies computed from the low-pass filtered GGM (referred to as *GGM height anomaly data set*) and (ii) height anomalies computed from the low-pass filtered model of equation (5) (referred to as *local height anomaly data set*). The low-pass filter coefficients are the ones of equation (4).

This sequential parameter estimation procedure is also used in this study. Details of the implementation of steps 1 and 2 are provided in Appendix A.

3. Data Sets and Stochastic Models

In this study, we use different local data sets, a satellite-only GGM, and a digital terrain model (DTM).

The *local data sets* comprise 411,947 radar altimeter-derived along-track QG height differences, 455,334 terrestrial gravity anomalies, 8.205 airborne gravity disturbances, and 94,137 shipboard gravity anomalies. These local data sets were complemented by 7,179 spatially interpolated gravity anomalies to fill areas void of data. Figure 1 shows a map of the data locations. The local data sets are essentially identical to the data sets used in Farahani et al. (2017a), except a number of improvements:

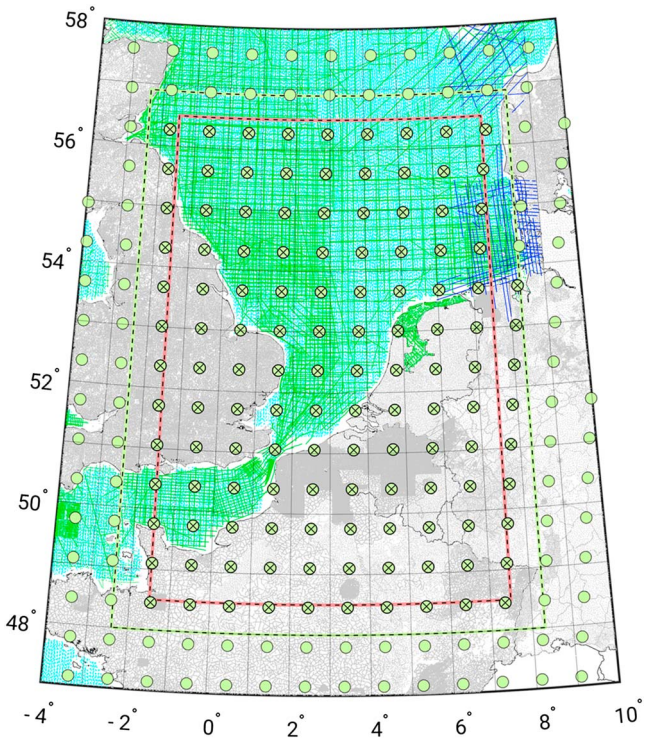

Figure 1. Map showing the outlines of the different areas used in this study and the locations of the data points: terrestrial gravity anomalies (gray), airborne gravity disturbances (blue), shipboard gravity anomalies (green), and radar altimetry data (cyan). The large yellow circles show that all locations of the data points at which the low-resolution height anomalies were computed from the global gravity model and local quasi-geoid model. The ones marked with a cross are the ones that were actually used in the combination. The yellow box shows the outline of area Ω_2 and the red box that of area Ω_T.

1. We removed a bug in the preprocessing of the Dutch terrestrial gravity data sets, which was caused by a wrong tidal correction applied to the Normaal Amsterdams Peil (NAP) heights.
2. We adjusted the telluroid heights of the gravity stations for vertical movements of NAP height markers as found in the fifth precise leveling campaign (Brand et al., 2004; Klees & Slobbe, 2018).
3. We adjusted the telluroid heights of the Belgian gravity stations for errors in the Belgian leveling network (TAW or Tweede Algemene Waterpassing) (Klees & Slobbe, 2018).
4. As shown in Klees and Slobbe (2018), the Belgian data sets have statistically significant biases ranging from −1.75 to 0.12 mGal of unknown origin. Therefore, we split the Belgian gravity anomaly data set into 23 subsets and estimated a bias parameter for each of them.
5. We recomputed the instantaneous dynamic topography (IDT) using the Dutch Continental Shelf Model version 6 (Zijl et al., 2013) now including the depth-averaged baroclinic pressure variations (Slobbe et al., 2013a), which were not included in Farahani et al. (2017a). The IDT is used to reduce the radar altimeter sea surface heights to the QG. To reduce long-wavelength orbit errors, the IDT-corrected radar altimeter sea surface heights are not used as observed QG heights but are used in the form of along-track QG height differences when computing the QG model.

The *satellite-only GGM* is the *regularized* GOCO05s GGM (Mayer-Gürr et al., 2015; Pail et al., 2010). The GOCO05s spherical harmonic model was low-pass filtered using the filter coefficients of equation (4). We refer to Klees et al. (2017) for the motivation of applying a low-pass filter. Then, height anomalies were synthesized at points on the Earth's surface, providing the GGM height anomaly data set. We followed Klees et al. (2017) and chose the low-pass filter parameters of equation (4) as $p_1 = 150$ (which is identical to the maximum spherical harmonic degree of the normal gravity field used in step 2 of the sequential parameter estimation procedure) and $p_2 = 230$. Hence, the GGM height anomaly data set (and the local height anomaly data set) does not contain any signal above degree 230. The choice of p_2 was driven by the height anomaly commission error of the regularized GOCO05s GGM. At degree 150, the commission error is just

0.8 cm. Beyond that degree, it increases rapidly to 3.2 cm at degree 200, 6.8 cm at degree 230, and 10.4 cm at the maximum degree 280; the signal-to-noise ratio is equal to 1 at degree 205. At the same time, the local data sets allow to compute height anomalies over the area of interest with a standard deviation (SD) of 1–2 cm; after low-pass filtering, the SD is at the millimeter level. Therefore, it does not make sense to include GOCO05s up to the maximum degree 280. On the other hand, using a value $p_2 < 280$ reduces the condition number of the noise VC matrix of the GGM height anomaly data set, which makes the computation of the weight matrix easier(Klees et al., 2018).

A *DTM* was used to compute the RTM corrections. Moreover, the DTM served as a model of the Earth's surface when generating the two height anomaly data sets used in step 2 of the sequential parameter estimation procedure. In this study, we used EuroDEM v1.0 (Hovenbitzer, 2008) that has a 2″ grid width. In areas where this model is not available, we used SRTM version 2.1 (Farr et al., 2007) with a 3″ grid width. For the remaining areas, we used ASTER GDEM v2 (Tachikawa et al., 2011) with a 1″ grid width.

Noise in terrestrial and shipboard gravity anomalies and airborne gravity disturbances was assumed to be zero mean white Gaussian. For the terrestrial gravity data sets, long-wavelength systematic and random errors were reduced by adding to the functional model a bias parameter per data set; a total of 133 bias parameters was included. For airborne gravity disturbances, Olesen et al. (2002) showed that noise correlations can be ignored if one aims at a 1-cm QG model. Though the SD of the QG model to be presented in section 5 appeared to be below 1 cm over the Netherlands, we had no access to the raw data and, therefore, had to refrain from modeling correlated noise in the airborne gravity disturbances. For shipboard data, the data preprocessing (in particular the along-track low-pass filtering and the crossover adjustment) introduces noise correlations. No study about the quantification of correlated noise in shipboard data is known to us. Due to a lack of information about the noise correlations introduced by the data preprocessing done by the data providers, we refrained from modeling the noise correlations introduced by the data preprocessing we did. Colored noise in the altimeter-derived data set was estimated using the method in Ditmar et al. (2007); see (Farahani et al., 2017a) for technical details of the implementation. To compute the noise VC matrix of the GGM height anomaly data set, we first computed the noise VC matrix of the regularized GOCO05s spherical harmonic model from the GOCO05s normal equation matrix N and the inverse of the regularized normal equation matrix, N_λ^{-1}, as $N_\lambda^{-1}NN_\lambda^{-1}$. The matrices N and N_λ^{-1} were provided by the GOCO team. Then, we computed the noise VC matrix of the GGM height anomaly data set using the law of covariance propagation. For each data set used in steps 1 and 2 of the sequential parameter estimation procedure, we estimated a variance factor using the minimum norm quadratic unbiased estimator (MINQUE; Rao, 1971). In doing so, we exploited the Monte Carlo method proposed by Koch and Kusche (2002) and Kusche (2003) in step 1. In step 2, the iterative MINQUE procedure was used. We refer to Appendix B for the results of the Monte Carlo variance component estimation (MCVCE).

4. Numerical Experiments

To answer the research questions of section 1, five different QG models were computed using the methodology and data sets described in sections 2 and 3, respectively.

1. Solution I uses the two-scale model of equation (1). It represents a statistically optimal (in the weighted least squares sense) combination of all data sets using the sequential parameter estimation approach of section 2.
2. Solution II uses the single-scale model of equation (5). The model parameters $\{d_{q,1}\}$ were estimated using the local data sets. Hence, solution II is a classical RCR solution.
3. Solution III uses the two-scale model of equation (1). The model parameters $\{d_{q,0}\}$ are computed using only the GGM height anomaly data set; the model parameters $\{d_{q,1}\}$ are computed using only the local data sets.
4. Solutions IV and V are similar to solution I, except that they use a simplified noise VC matrix for the GGM height anomaly data set. The simplified noise VC matrix used in solution IV is obtained by covariance propagation of the *diagonal* elements of the noise VC matrix of the GGM's spherical harmonic coefficients (note that it is still a full matrix). The motivation for including solution IV in the analysis is that it uses the same stochastic information about the noise in the GGM as was used in the computation of the European QG Model EGG2015 (Denker, 2015). Though EGG2015 uses a Stokes integral-based method of QG modeling, solution IV will provide information about the impact on the computed QG model of using

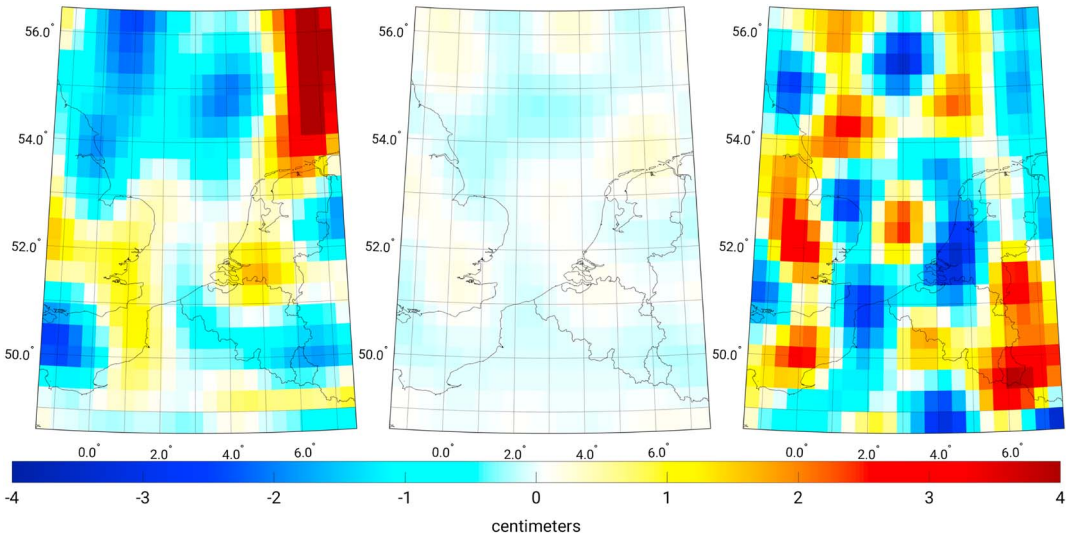

Figure 2. Differences between quasi-geoid (QG) solution I and (i) QG solution II (left panel), (ii) QG solution IV (middle panel), and (iii) QG solution V (right panel).

incomplete information about the noise in the GGM. Solution V uses only the diagonal elements of the full GGM height anomaly data set's noise VC matrix used in computing solution I. The motivation for including solution V is that most methods and software used in local QG modeling cannot deal with an ill-conditioned noise VC matrix. As shown in Klees et al. (2018), the noise VC matrix of the GOCO05s GGM height anomaly data set has a condition number of about 10^{16}. Dealing with this ill-conditioned matrix in weighted least squares requires the use of one of the methods suggested in Klees et al. (2018). For information about the method used in this study, we refer to Appendix A.

5. Results and Discussion

Here we present, discuss, and compare the five QG solutions of section 4 to each other and to EGG2015 and validate them using GPS/leveling data as control data sets. Two GPS/leveling data sets are available, from which so-called "geometric height anomalies" can be computed. The Belgium data set comprises 3,760 points and has a mean noise SD of about 11 mm. The data set over the Netherlands comprises 82 points and has a mean noise SD of about 5.8 mm. For further details about the control data sets, we refer to Appendix C. Additional information about the computation of the solutions I–V is provided in Appendix B.

5.1. The Impact of a Noisy GGM on a Local QG Model

To answer the main research questions of section 1, we compare QG solutions I and II and assess their quality using the GPS/leveling control data sets.

The left panel of Figure 2 shows a spatial rendition of the differences between QG solutions I and II. The largest absolute difference shows up in the northeast corner of the model domain, Ω_T; here the differences reach −5.2 cm. Over Belgium and the Netherlands, the differences are between −1.5 and 1.5 cm.

Table 1 shows the statistics of the differences of QG solutions I and II, respectively, to the GPS/leveling control data sets. For Belgium, the SD is 1.52 cm for QG solution I compared to 1.62 cm for QG solution II. For the Netherlands, the situation is the opposite, 0.95 cm for QG solution I versus 0.66 cm for QG solution II. Given the quality of the control data sets (the mean SD for the control data set is about 0.58 cm for the Netherlands and 1.10 cm for Belgium; see Appendix C), it is difficult to judge whether the statistics point to a superior quality of QG solution II compared to QG solution I. For instance, a statistical analysis of the differences between the gravimetric and geometric height anomalies over the Netherlands shows that only six out of 82 differences are statistically different from zero at the 95% confidence level.

Information about the quality of QG solution I compared to QG solution II as function of the spatial scales is provided by a variogram analysis of the differences with respect to the GPS/leveling control data sets. Figure 5 shows the empirical variograms for the QG solutions I–V. Each variogram represents the variance of the differences between a QG solution and the GPS control data set for pairs of points as a function

Table 1
Statistics of the Differences Between Geometric and Gravimetric Height Anomalies at the GPS/Leveling Stations for the Five QG Solutions of Section 1 and EGG2015

Solution	Control data set	RMS (cm)	Range (cm)	Mean (cm)	SD (cm)
I	Belgium	2.28	13.1	1.7	1.52
II		2.17	13.9	1.4	1.62
III		2.83	14.4	2.0	1.96
IV		2.29	13.2	1.7	1.52
V		2.77	14.5	2.0	1.96
EGG2015		1.64	13.0	−0.1	1.64
I	NL	1.17	4.2	−0.7	0.95
II		0.69	3.5	−0.2	0.66
III		2.31	8.2	−1.4	1.87
IV		1.11	4.0	−0.6	0.91
V		2.26	7.5	−1.4	1.77
EGG2015		3.73	5.1	−3.6	0.96

Note. The control data sets comprise 3,760 (Belgium) and 82 (NL) points, respectively. QG = quasi-geoid; NL = Netherlands; RMS = root mean square.

of the lag distance. After Bachmaier and Backes (2011), we use the term "gammavariance" to refer to the variance of the differences at a given lag distance. As the differences among the QG solutions I–V are all of long-wavelength nature (at a latitude of 50°, degree $p_1 = 150$ corresponds to 55 km and degree $p_2 = 230$ to 85 km half-wavelength resolution), we expect that the variograms may differ mainly at lag distances above 55–85 km.

When comparing the empirical variogram of QG solution I with the one of QG solution II, we observe that the former has significantly lower gammavariances for lag distances >100 km over Belgium. Over the Netherlands, we observe slightly larger gammavariances for QG solution I for all lag distances >30 km. This indicates that over Belgium a weighted least squares combination of GOCO05s with the local data sets improves the quality of the QG model significantly, whereas a slight deterioration is observed over the Netherlands. The latter is a direct consequence of the results of the variance component estimation (VCE) applied in step 2 of the sequential parameter estimation procedure. As shown in Appendix B, VCE increases the SD of the local height anomaly data set from 0.068 to 1.52 cm, whereas the SD of the GOCO05s height anomaly data set slightly decreases from 2.5 to 2.28 cm. Hence, VCE downweights the local height anomaly data set relative to the GGM height anomaly data set by a factor of about 600. We refer to Appendix B for a discussion about the downweighting of the local height anomaly data set.

The gammavariances over the Netherlands behave differently from those over Belgium. There may be several reasons for that. For instance, the Dutch terrestrial and shipboard gravity data sets were measured in the eighties of the last century with the aim to compute a new QG model. Measurement setup and data preprocessing followed well-defined standards, providing homogeneous, high-quality data sets. At the same time, the lack of topography guarantees that no high-frequency signal is left in the data after RTM correction. For Belgium, the situation is different. The terrestrial gravity data sets origin from numerous sources, the data acquisition was spread over decades, the gravity data were not acquired specifically for QG modeling, and the gravity data in the hilly areas still contain some spurious high-frequency signals after RTM correction. The significant bias parameters for various subsets of the Belgium gravity data sets documented in Klees and Slobbe (2018) support this interpretation.

The statistics of the fit of QG solution I to the GPS/leveling control data sets are slightly better over Belgium than those of EGG2015 (cf. Table 1); the SD of the differences to the GPS/leveling data is 1.52 cm for QG solution I and 1.64 cm for EGG2015. Over the Netherlands, the summary statistics are almost the same (SD of 0.95 cm for QG solution I versus 0.96 cm for EGG2015). The geographic plot of the differences of Figure 3 shows, however, significantly different spatial patterns. The variograms of Figure 5 provide additional information about the performance of EGG2015 as function of the spatial scales. They reveal a comparable accuracy of EGG2015 compared to QG solution I up to 100 km (Belgium) and 120 km (the Netherlands),

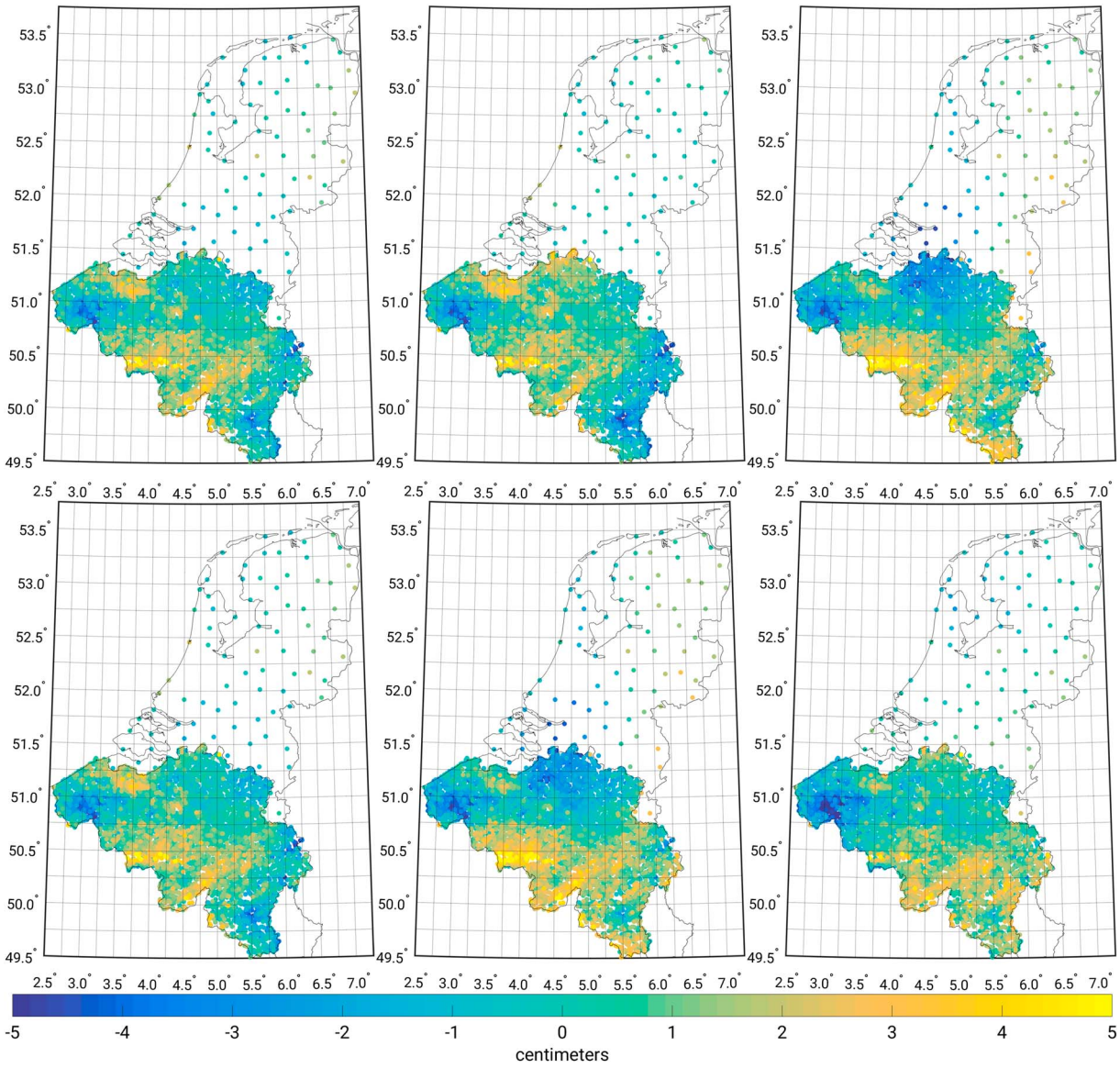

Figure 3. Differences between geometric and gravimetric height anomalies at the GPS/leveling stations. Top row from left to right: quasi-geoid solutions I, II, and III. Bottom row from left to right: quasi-geoid solutions IV, V, and EGG2015.

respectively. For larger lag distances, however, the EGG2015 gammavariances increase rapidly and exceed those of QG solution I. Hence, QG solution I is better than EGG2015 at these spatial scales.

5.2. The Impact of Using Exclusively the GGM Height Anomaly Data Set to Model the Coarse Scales of the QG

The impact of using the GOCO05s height anomaly data set to determine the coarse scales of the QG model is assessed by comparing QG solutions II and III. These solutions differ in the coarse scales, which are obtained from either the local data sets (solution II) or the GGM height anomaly data set (solution III). Figure 4 shows a spatial rendition of the differences between QG solutions II and III. The differences range from −6.1 to 4.8 cm; the SD is 2.3 cm. They provide an upper bound of the impact of the GOCO05s GGM on the computed QG model.

Table 1 shows the statistics of the differences between QG solutions II and III, respectively, and the GPS/leveling control data sets. According to these statistics, QG solution III has a significantly poorer fit compared to QG solution II. The poorer fit is very pronounced over the Netherlands; the range and SD of the differences increase from 3.5 and 0.66 cm (QG solution II) to 8.2 and 1.87 cm (QG solution III), respectively.

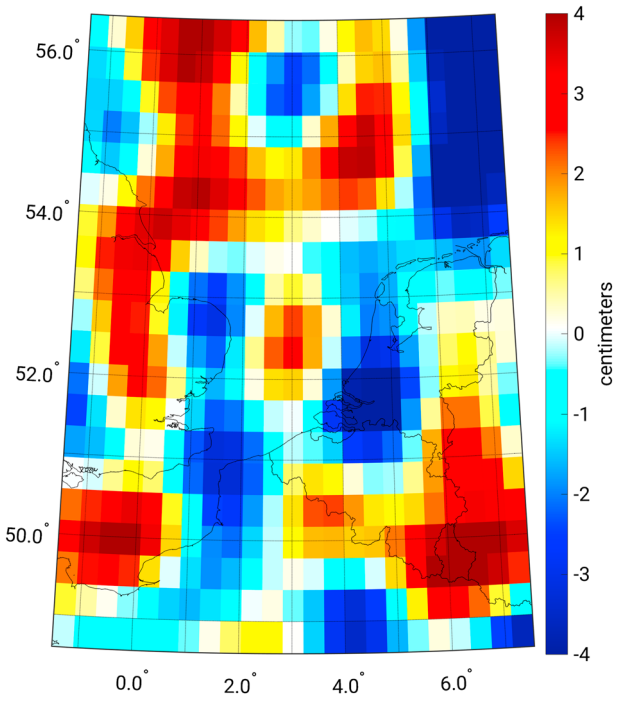

Figure 4. Spatial rendition of the differences between quasi-geoid solutions II and III. The plot gives an impression of the maximum impact of the global gravity model height anomaly data set on the quasi-geoid model.

For Belgium, the statistics do not differ that much; the range increases from 13.9 cm (QG solution II) to 14.4 cm (QG solution III), and the SD increases from 1.62 cm (QG solution I) to 1.96 cm (QG solution III). This shows that at the scales resolved by the GOCO05s height anomaly data set, the local data sets are overall of a higher quality compared to the GOCO05s height anomaly data set.

A spatial rendition of the differences with respect to the GPS/leveling control data sets, which is shown in Figure 3, provides additional information about the quality of QG solution III compared to QG solution II. First of all, we notice that the differences of QG solution III to the GPS/leveling control data set are particularly large in the area around 51.75°N and 4.5°E. This reduced fit, which spreads across the Belgian border, has a relatively strong impact on the statistics over the Netherlands, because this control data set comprises only 82 GPS/leveling stations. Second, there are also areas where QG solution III shows a better fit to the GPS/leveling control data compared to QG solution II. For instance, along the border of Belgium to Germany and Luxembourg, the differences are between 1 and 2 cm for QG solution III compared to −1 to −5 cm for QG solution II. This shows that in this area, the GOCO05s GGM improves the QG model.

Figure 5 reveals that the gammavariances of QG solution II are significantly lower than those of QG solution III for all lag distances above, say, 20–30 km for the Netherlands and Belgium. This provides evidence that QG solution II is superior to QG solution III, which was in particular for Belgium not that pronounced from the SDs of the differences presented in Table 1 (the SDs just differ by 0.34 cm). The behavior of the gammavariances as a function of the lag distance is, however, not the same for both countries. For Belgium, the gammavariances of QG solution III increase faster than those of QG solution II up to lag distances of 100 km. Between lag distances of 100 and 175 km, the differences between the gammavariances reduce before they start increasing again. This behavior of the gammavariances of QG solution III relative to the ones of QG solution II indicates that over Belgium, GOCO05s has a positive effect on the QG model. For the Netherlands, the gammavariances of QG solution III relative to the ones of QG solution II increase more or less continuously up to a lag distance of about 185 km, after which they start decreasing. We explain the decrease beyond lag distances of 185 km by the fact that 185 km is approximately the maximum east-west extension of the Netherlands. Up to this lag distance the

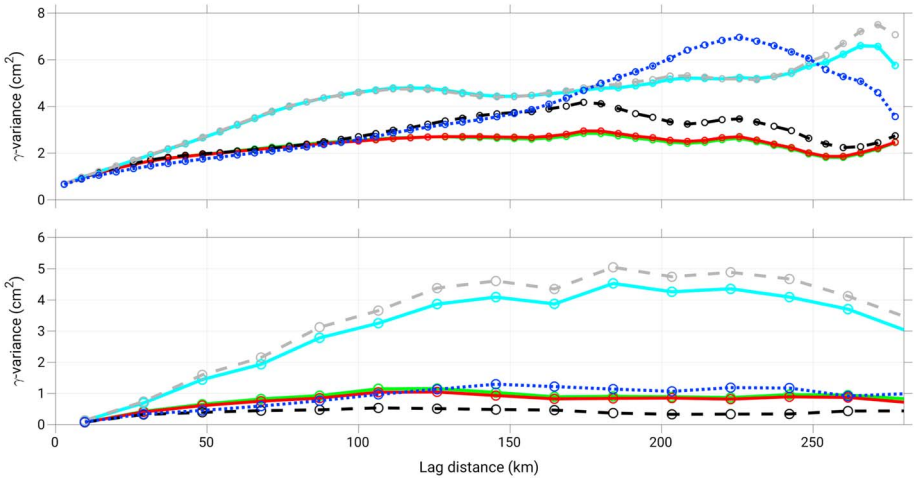

Figure 5. Variogram of the differences between geometric and gravimetric height anomalies at the GPS/leveling stations in Belgium (top panel) and the Netherlands (bottom panel) for solution I (green solid line), solution II (dashed black line), solution III (dashed gray line), solution IV (red solid line), solution V (cyan solid line), and EGG2015 (dotted blue line).

variogram is omnidirectional. For larger lag distances, the gammavariances are dominated by point pairs in north-south direction. The quality of the GGM height anomaly differences is better in the north–south direction than in east-west direction, due to the dominant contribution of the GRACE satellites to the GOCO05s GGM at these wavelengths. We can exclude that the decrease is caused by an insufficient number of data to compute the gammavariances at the long wavelengths. Though the number of pairs available to compute the gammavariances decreases for lag distances above 110 km, there are still 75 pairs available to compute the gammavariances at a lag distance of 250 km.

5.3. The Impact of Using a Simplified Noise VC Matrix for the GGM Height Anomaly Data Set

The impact of using a simplified noise model for the GOCO05s height anomaly data set on the computed QG model is assessed by comparing solution I with solutions IV and V, respectively.

The results of the VCE applied in step 2 of the sequential parameter estimation procedure (see Table B2 of Appendix B) show that the estimated variance factors of the GGM height anomaly data set and the local height anomaly data set, respectively, are quite similar for QG solutions I and IV (0.83 versus 0.81 and 509.9 versus 477.9, respectively). This implies an only marginal change in the relative contribution of each data set to the QG model; the contribution of the GGM height anomaly data set to the QG model is larger for QG solution I compared to QG solution IV. The effect this has on the computed QG model is very small; the differences range from −2.5 to 3.2 mm. These small differences hardly affect the statistics of the differences with respect to the GPS/leveling control data sets. We only observe a slightly better fit of QG solution IV to the GPS/leveling data over the Netherlands. This can be explained by the fact that the local height anomaly data set is slightly less downweighted in QG solution IV compared to QG solution I, which brings the former a bit closer to QG solution II.

The variance factors and posteriori SDs for QG solution V differ significantly from those of QG solution I: 0.83 versus 0.01 for the GGM height anomaly data set and 509.9 versus 5919.5 for the local height anomaly data set. This relative weighting of the two data sets implies that the coarse scales of the QG solution V are almost completely determined by the GGM height anomaly data set. This also explains why QG solution V is very close to QG solution III. Moreover, it shows that when combining a noisy GGM with noisy local data sets, the computed QG model is very sensitive to the noise VC matrices of the involved data sets and the estimated variance factors in step 2 of the sequential parameter estimation procedure.

6. Summary and Conclusions

In this study, we presented, applied, and validated a local QG model for the Netherlands, Belgium, and southern North Sea. It was computed from a satellite-only GGM and local data sets using weighted least squares techniques. The combination of a noisy satellite-only GGM with noisy local data sets goes beyond the classical RCR technique, which does not use the GGM in the same way as the local data sets. Our approach differs from others published in the literature in two respects. First, we do consider a state-of-the-art satellite-only GGM, which uses among others GRACE and Gravity field and steady-state Ocean Circulation Explorer (GOCE) data. Second, we used realistic noise models for all involved data sets; in particular, we used a full noise VC matrix for the GGM data set. As the resolution of the GGM is significantly different from that of the local data sets, we used a two-scale SRBF model of the disturbing potential. The scale-dependent model parameters were estimated sequentially to reduce signal leakage.

Overall, four research questions were addressed. The two main research questions were related to the impact of using a satellite-only GGM as one of the noisy data sets on the estimated QG model and to the quality of this model compared to a classical RCR QG model. To answer the first question, we compared a RCR QG model (QG solution II) to a QG model in which all data sets (including the GGM height anomaly data set) were considered as noisy data sets (QG solution I). Particularly, the noise VC matrix of the GGM height anomaly data set was propagated from the full noise covariance matrix of the GGM's spherical harmonic coefficients using the law of covariance propagation. All data sets were combined using weighted least squares. The differences between QG solutions I and II appeared to be significant with a range of 7.8 cm and a SD of 1.34 cm over the model domain. Over Belgium and the Netherlands, the differences are between −1.5 and 1.5 cm. A comparison with GPS/leveling control data sets showed a slight improvement of the QG's quality over Belgium (the SD of the differences improves from 1.62 to 1.52 cm) but a slight deterioration over the Netherlands (the SD of the differences increases from 0.66 to 0.95 cm). The corresponding empirical variograms showed a significant reduction of the gammavariances for lag distances > 100 km over

Belgium in favor of QG solution I. For the Netherlands, we observed marginally larger gammavariances over all lag distances > 30 km for QG solution I. This result is determined by the outcome of the VCE used in step 2 of the sequential parameter estimation procedure, which does the combination of the GGM with the local data sets at the spatial scales resolved by the GGM. The VCE downweighted the local data sets relative to the GGM by a factor of about 600. Whether this strong downweighting is realistic or triggered by the ill-conditioned noise VC matrix of the GGM data set is the subject of ongoing research. Anyway, the results illustrate the importance of VCE when combining the GOCO05s GGM with local data sets.

Two additional research questions were addressed. First, we assessed the impact of using exclusively the GOCO05s GGM to determine the coarse scales of the QG model (QG solution III). We showed that this solution differs significantly from a RCR QG model (QG solution II) with a peak-to-peak difference of 10.9 cm. We also showed that QG solution III provides a worse fit to the GPS/leveling control data sets. Over Belgium, the SDs increased from 1.62 cm (QG solution II) to 1.96 cm (QG solution III). Over the Netherlands, they increased from 0.66 cm (QG solution II) to 1.87 cm (QG solution III). This poor performance of QG solution III was also confirmed by the variogram analysis. At *all* lag distances, the gammavariances of QG solution III were larger than those of QG solution II. From a spatial rendition of the differences, we found that only in the eastern part of Belgium, GOCO05s slightly improved the quality of the computed QG model.

Finally, we quantified the impact on the computed QG model of using simplified noise models for the GGM height anomaly data set (research question 4). Here two alternative scenarios were considered. In the first alternative, we used the diagonal noise VC matrix of the GGM's spherical harmonic coefficients to compute the noise VC matrix of the GGM height anomaly data set by applying the law of covariance propagation (QG solution IV). We found that the simplified noise VC matrix led to a slightly larger contribution of the local data sets to the spatial scales resolved by the GGM compared to QG solution I, leading to differences between both QG solutions of a few millimeters. From this we conclude that the noise covariances of the GOCO05s spherical harmonic model had a limited impact on the computed QG model.

In the second alternative, we propagated the full noise covariance matrix of spherical harmonic coefficients into the GGM height anomaly data set but used only the diagonal elements of the latter when computing the QG model (QG solution V). We found that in this case, VCE assigned extremely small weights to the local height anomaly data set, making the contribution of this data set to the QG model at the spatial scales resolved by the GGM negligible.

We would like to conclude with two remarks. First, a proper interpretation of the results presented in this study requires to remember that the gravity anomaly data sets used in this study are of high quality compared with the quality of gravity anomaly data sets in many areas around the world. This applies in particular to the data sets over the Netherlands, which have a dense, homogeneous coverage, a very low noise SD of better than 0.5 mGal, and do not suffer from systematic errors. Moreover, in all QG solutions computed in this study, we estimated bias parameters for all gravity data sets (except the ones over the Netherlands). A total of 133 of them appeared to be statistically significant. In this way, long-wavelength systematic and random errors in these data sets could be reduced significantly. Though many of these data sets cover only small areas (often smaller than the spatial resolution of GOCO05s), they introduce long-wavelengths systematic errors in the computed QG model as shown in Klees et al. (2018). Without these bias parameters, the quality of the computed QG models would be much lower, though the combination with GOCO05s would partially compensate for the biases in the largest data sets. Most areas of the world lack high-quality, dense terrestrial gravity anomaly data sets. In these areas, the impact of the GOCO05s GGM on the estimated QG model would be larger than shown here.

Second, we would like to highlight that the quality of the QG solutions we computed in this study approached the quality of the GPS/leveling control data sets (in particular over the Netherlands). Given the formal errors of the gravimetric and geometric height anomalies, we found that only six out of the 82 differences between gravimetric and geometric height anomalies over the Netherlands are statistically significant. Given the growing interest in computing QG models with a SD of 1 cm or better, our findings underscore the need for a better or a new type of control data set to validate QG models. These may be obtained by (i) using better GNSS solutions, for example, use multi-GNSS and increase the visiting time per station; (ii) improving the quality of the heights at the height markers, in particular reduce the magnitude of the systematic errors still present in many height networks all around the world; and (iii) using QG profiles measured with CCD cameras as alternative control data set (e.g., Hirt & Seeber, 2008). The validation at sea is even more challenging. The

quality of water levels provided by a hydrodynamic model and coastal distortions in the mean sea surface from radar altimeter data rendered any attempt of QG model validation in the southern North Sea useless.

Appendix A: Sequential Estimation of the Model Parameters

In the following, we describe the implementation of the sequential model parameter estimation approach of section (2) for real data sets. Moreover, we present the main choices we made when processing the data.

A1. Estimation of the Model Parameters $\{d_{q,1}\}$

The parameters $\{d_{q,1}\}$ of the two-scale model of the disturbing potential, equation (1), were estimated from the local data sets using the RCR technique and weighted least squares. The GGM GOCO05s complete to degree 280 was used as the normal gravity field.

Edge effects and computation domain. Edge effects are a well-known problem when computing a local QG model. To control them, the data area is commonly chosen larger than the area of interest. This poses some constraints to the sequential estimation approach. The single-scale model of the disturbing potential, equation (5), is used to generate one of the data sets used in step 2. Therefore, the domain of the single-scale model, say Ω_2, must be chosen larger than the area of interest, Ω_T. To compute a model over a domain Ω_2 requires data to be available over an even larger domain, say Ω_1. Hence, the high-resolution local data sets, which are used to estimate the single-scale model of the disturbing potential, must be available over an area Ω_1, where $\Omega_T \subset \Omega_2 \subset \Omega_1$.

The area of interest, Ω_T, is bounded by 48.5°N to 56.5°N and 1.5°W to 7.5°E. It comprises the entire Netherlands, Belgium, and the southern North Sea. Based on a comparison to the European QG EGG2015 (not shown here), we computed QG model estimates, for different choices of Ω_1 and Ω_2. We found that edge effects in the computed QG model are below the noise level when Ω_1 is chosen as 47°N to 58°N and 4°W to 10°E, and Ω_2 is chosen as 48°N to 56.9°N and 2.4°W to 8.3°E.

RCR technique. The single-scale model of equation (5) is computed using the procedure outlined in Slobbe (2013) and Farahani et al. (2017a) with some modifications. To reduce linearization and spherical approximation errors in the functional model of the local data sets and to reduce the long-wavelength signal content in the data sets, we use the GOCO05s GGM (Mayer-Gürr et al., 2015; Pail et al., 2010) complete to degree 280 as the normal gravity field (e.g., Denker, 2013). The very short wavelengths in the data, which the data density does not allow to resolve and which for that reason is not included in the model of equation (5), are removed from the data using RTM (e.g., Forsberg, 1984). The RTM surface was obtained by applying a circular sharp cutoff filter with a full width of 180°/280 (here, 280 is the maximum degree of the normal gravity field) to a coarse DTM surface. The latter was obtained by applying a blockmean filter with a width of 0.05°× 0.05° to the DTM used in this study (see section 3). The RTM corrections were computed using the method of Heck and Seitz (2007). Bathymetry was not considered when computing the RTM correction. Its contribution to the RTM correction is negligible over Ω_1 as both water depths and slopes in bathymetry are small in the southern North Sea. Ignoring the bathymetry contribution reduces the numerical costs significantly, among others, because we do not have to compute RTM corrections for the radar altimeter-derived along-track QG height differences.

Parameterization. The domain of the model of equation (5) is Ω_1. The SRBFs used in this study are Poisson wavelets of order 3 (Holschneider & Iglewska-Nowak, 2007); that is, the Legendre coefficients ϕ_l of equations (2), (3), and (6) are given as $\phi_l = l^3$. The parameter L_T of equation (3) depends on the available data sets, in particular the data density, distribution, and signal-to-noise ratio. For the data sets available in this study, a representative mean value is $L_T = 10,000$. In this study, we used $L_T = \infty$. Test computations reveal that this has a negligible influence on the computed QG model, at the benefit of using analytical expressions for the computation of the SRBFs of equation (6), which are given in Holschneider and Iglewska-Nowak (2007). This makes the computation of the design matrix numerically much more efficient. The analytical expressions of the SRBFs for the gravity field functionals used in this study are given in Tenzer and Klees (2008). The SRBFs are positioned below the data points that are closest to the nodal points of a Fibonacci grid (González, 2010). This is different from Farahani et al. (2017a), who positioned the SRBFs on a Fibonacci grid. The advantage of the approach pursued here is that all SRBF coefficients are well constrained by the data. We found that following Farahani et al. (2017a) may result in poorly estimated model parameters for the data sets used in this study causing local distortions in the computed QG model. We use the procedure in Slobbe

(2013) to find suitable values for the location of the SRBFs. The set of SRBFs is complemented with bias parameters for the terrestrial, shipboard, and airborne gravity data to account for existing inconsistencies among various gravity data sets. Such inconsistencies are, for instance, caused by unknown gravity/height datum offsets (Klees & Slobbe, 2018).

Least squares estimation and data weighting. The model parameters and the bias parameters were estimated using weighted least squares with zero-order Tikhonov regularization (Tikhonov, 1963) confined to the SRBF model parameters. We used the method in Wittwer (2009) to find a suitable regularization parameter.

The outcome of step 1 is estimates $\{\hat{d}_{q,1}\}$ of the model parameters $\{d_{q,1}\}$ and bias parameters for the local gravity data sets with full dispersion matrix.

A2. Estimation of the Model Parameters $\{d_{q,0}\}$

The parameters $\{d_{q,0}\}$ of the model of equations (1) and (7), respectively, were estimated from the GGM height anomaly data set and height anomaly data set synthesized from the model of equation (5) and low-pass filtered (local height anomaly data set; see section 2).

Data sets. The first step in the estimation of the coarse-scale model coefficients $\{d_{q,0}\}$ is the generation of the two low-pass filtered height anomaly data sets over the domain Ω_2 including full noise VC matrices: (i) height anomalies from the spherical harmonic model of the GGM (to be referred to as *the GGM height anomaly data set*) and (ii) height anomalies from the estimated model of equation (5) (to be referred to as *the local height anomaly data set*). The low-pass filter of equation (4) is applied to the spherical harmonic model of the GGM and the estimated model of equation (5) prior to the generation of the height anomaly data sets, providing the height anomaly data sets used to estimate the model coefficients $\{d_{q,0}\}$. Both height anomaly data sets were generated on the Earth's surface (represented by the DTM) at the nodes of a Reuter grid (Reuter, 1982) with control parameter N, which determines the density of the grid. By assessing the model error obtained using noise-free data generated at a number of Reuter grids with different control parameters starting from $N = p_2 + 1$, we found that at least $1.2 \times (p_2 + 1)$ grid nodes are needed to achieve a model error that is negligible (order of millimeters) compared to the data noise (order of centimeters).

Generation of the height anomaly data sets. The GGM height anomaly data set comprises height anomalies computed at the nodes of the data grid by spherical harmonic synthesis of the spherical harmonic model of the GOCO05s GGM. Before synthesis, the spherical harmonic coefficients were low-pass filtered using the filter coefficients of equation (4) with parameters $p_1 = 150$ and $p_2 = 230$. The height anomalies were referenced to the potential value of the European Vertical Reference Frame 2007 (EVRF2007) zero level surface, that is, $W_0^{(\mathrm{EVRF2007})} = 62,636,857.89 \pm 0.02\ \mathrm{m}^2/\mathrm{s}^2$ (Denker, 2013). To generate the local height anomaly data set, we used the model of equation (5), which was computed in step 1 of the sequential estimation procedure and applied the filter coefficients of equation (4) with the same parameters $p_1 = 150$ and $p_2 = 230$. We added the low-pass filtered RTM corrections, which were computed by applying the low-pass filter of equation (4) in the spatial domain to the RTM correction in terms of height anomalies at the nodes of the data grid. Finally, we restored the low-pass filtered height anomalies of the GOCO05s GGM from degrees 151 to 280 to account for the different normal gravity fields used in steps 1 and 2, respectively. The noise VC matrices of the two height anomaly data sets were obtained by applying the law of covariance propagation to the full noise VC matrix of the spherical harmonic coefficients and the VC matrix of the estimated model parameters $\{d_{q,1}\}$, respectively.

Bias removal. The final preprocessing step consists of removing the bias between the two low-pass filtered height anomaly data sets to ensure that W_0^{EVRF2007} is the datum of the computed QG model. The bias was computed as the weighted average of the differences between the two data sets, where the weights correspond to the cosine of the datapoint's latitude.

Parameterization. The optimal depth of the SRBFs of equation (7) was found by assessing the model error at a height anomaly control data set in case only one data set was used.

Least squares estimation and data weighting. The functional model for the two height anomaly data sets can be written as a linear Gauss-Markov model

$$E\{\mathbf{y}_j\} = \mathbf{A}_j\mathbf{d}, \quad D\{\mathbf{y}_j\} = \mathbf{C}_j = \sigma_j^2\mathbf{Q}_j, \ j = 1, 2, \tag{A1}$$

where E is the expectation operator and D is the dispersion operator, $\mathbf{y}_j$ is the vector of height anomalies of observation group j, $\mathbf{A}_j$ is the design matrix of observation group j, $\mathbf{d}$ is the vector of model parameters $\{d_{q,0}\}$, $\mathbf{C}_j$ is the height anomaly noise VC matrix of observation group j, $\mathbf{Q}_j$ is the cofactor matrix of observation group j, and σ_j^2 is the variance factor of observation group j. With

$$\mathbf{y} = \begin{pmatrix} \mathbf{y}_1 \\ \mathbf{y}_2 \end{pmatrix}, \mathbf{A} = \begin{pmatrix} \mathbf{A}_1 \\ \mathbf{A}_2 \end{pmatrix}, \mathbf{C} = \begin{pmatrix} \sigma_1^2\mathbf{Q}_1 & \mathbf{0} \\ \mathbf{0} & \sigma_2^2\mathbf{Q}_2 \end{pmatrix}, \tag{A2}$$

the Gauss-Markov model of equation (A1) is written as

$$E\{\mathbf{y}\} = \mathbf{A}\mathbf{d}, \quad D\{\mathbf{y}\} = \mathbf{C}. \tag{A3}$$

The inversion-free weighted least squares estimator (e.g., Grafarend & Schaffrin, 1993) of the vector of model coefficients α is defined as

$$\hat{\mathbf{d}} = \mathbf{A}'\left(\mathbf{A}\mathbf{A}' + \mathbf{C}\mathbf{B}\mathbf{C}\right)^{-1}\mathbf{y}, \tag{A4}$$

where

$$\mathbf{B} = \mathbf{I} - \mathbf{A}\left(\mathbf{A}'\mathbf{A}\right)^{-1}\mathbf{A}'. \tag{A5}$$

In the numerical experiments of section 5, we needed to apply some regularization to the matrix $\mathbf{A}\mathbf{A}' + \mathbf{C}\mathbf{B}\mathbf{C}$ in equation (A4) and the matrix $\mathbf{A}'\mathbf{A}$ in equation (A5). We used Tikhonov regularization with a unit regularization matrix. The two regularization parameters were chosen such that the amount of regularization applied to both matrices is the same, that is,

$$\lambda = \lambda_{\text{eff}}\frac{\text{Tr}(\mathbf{A}\mathbf{A}' + \mathbf{C}\mathbf{B}\mathbf{C})}{m}, \quad \lambda' = \lambda_{\text{eff}}\frac{\text{Tr}(\mathbf{A}'\mathbf{A})}{n}, \tag{A6}$$

where m is the number of observations, n is the number of parameters, and λeff is the *effective regularization parameter*.

The two variance factors σ_1^2 and σ_2^2 were estimated using the iterative MINQUE (Rao, 1971). The iteration was terminated when the relative change of successive variance factors for both observation groups was smaller than 10^{-4}.

Once the model parameters $\{d_{q,0}\}$ and $\{d_{q,1}\}$ have been computed, the two-scale model of the residual disturbing potential is given by equation (1). This model can be used to compute residual height anomalies at any point inside the area of interest, Ω_T. To obtain the full height anomaly signal, we needed to restore the height anomaly signal of (i) the normal field used in step 2 (GOCO05s complete to degree 150), (ii) the high-pass filtered normal field used in step 1 (GOCO05s complete to degree 280), and (iii) the RTM correction. Whereas the computation of (i) and (ii) was straightforward, (iii) was not, as the height anomaly RTM correction is only known at the location of the local data sets used in step 1. In principle, one could interpolate the height anomaly RTM corrections at any point inside Ω_T, hoping that they are smooth enough to avoid significant interpolation errors. Here we decided against any interpolation. Therefore, the full high-resolution QG model of equation (1) was evaluated at the locations of the local data sets. The height anomaly RTM correction we had to restore was the difference between the full height anomaly RTM correction (computed in the data preprocessing of step 1) and the low-pass filtered height anomaly RTM correction (already restored in step 2). This difference was then restored at the locations of the local data sets of step 1. The final result is a high-resolution local QG model defined at the location of the local data sets. For further processing, this model was then interpolated on an equal-angular grid.

Appendix B: Additional Information About the Computation of QG Models I–V

To compute the QG models I–V, we had to determine the density of the grid that defines the initial locations of the basis functions $\Psi_{q,1}$ of equation (1) and $\Phi_{q,1}$ of equation (6). This density, expressed in terms of the distance between the grid nodal points, was 10 km at sea and 4 km on land resulting in a total number of 46,234 SRBFs. The optimal depth of the SRBFs at sea and land was found to be 40 and 25 km below the RTM surface, respectively. In total, 133 bias parameters were estimated together with the SRBF model parameters to account for systematic and long-wavelength random errors in the gravity data sets. The results of the MCVCE applied to estimate the weights of the individual high-resolution data sets are summarized in

Table B1
A Posteriori Standard Deviations (SDs) of Terrestrial, Shipboard, and Interpolated Gravity Anomalies, Airborne Gravity Disturbances, and Altimeter-Derived Along-Track QG Height Differences for all ERM and GM Altimeter Mission Phases Used in the Computation of T_1

Data	Mission phase	Number of data points	A posteriori SD (cm)	A posteriori SD (mGal)
Terrestrial		453,334		0.70
Shipboard		94,137		1.23
Interpolated data set		7,179		0.50
Airborne		8,205		1.33
Radar altimetry	CryoSat-2	192,117	3.54	5.54
	ERS1BD	404	1.02	1.54
	ERS1CG+ERS2+EnvisatB+SA	4,621	1.73	2.51
	ERS-1 (phase A)	356	2.48	3.75
	ERS-1 (phase E)	18,744	4.23	6.39
	ERS-1 (phase F)	18,755	4.84	7.31
	Envisat (phase C)	54,960	2.65	3.52
	GFO-1	2,914	2.18	3.27
	Geosat (phase D)	68,724	3.28	4.92
	Jason-1 (phase B)	1,723	0.99	1.68
	Jason-1 (phase C)	53,766	3.01	5.16
	TopexA+Poseidon+Jason1A+Jason2	1,767	1.12	1.87
	TOPEX (phase B)	1,460	0.88	1.40
	TOPEX (phase N)	4,796	2.83	4.52

Note. The SDs for the altimeter-derived data sets were converted from units of centimeters to units of milligal using the rule of thumb that 1 μrad geoid slope corresponds to 1 mGal gravity anomaly; see, for example, Sandwell and Smith (1997) and Smith (2010). They should only be used to support a comparison of the relative weighting of the altimeter-derived data set and the shipboard gravity data set. SD = standard deviation.

Table B1. Even though the parameterization and used data sets are slightly different compared to the ones used in Farahani et al. (2017a), the obtained a posteriori SDs in both studies are very similar for all observation groups. Just taking the main gravity data sets as an example, we obtained 0.70, 1.23, and 1.33 mGal for, respectively, the terrestrial, shipboard, and airborne data sets. Farahani et al. (2017a) reported 0.73, 1.15, and 1.36 mGal. The relatively low a posteriori SD for the interpolated data set is explained by the fact that these data points were added in locations void of data to guarantee that all SRBF model parameters can be estimated. Hence, the residuals at the interpolated data are pretty small. In general, the obtained a posteriori SDs are realistic for *todays* instruments. However, most terrestrial gravity data sets were acquired decades ago. The same applies to the shipboard gravity data; most were acquired before the GNSS era. Hence, the a posteriori SDs for these data sets are believed to be too optimistic. The mutual ratios are, however, reasonable. For a more in-depth analysis of these MCVCE results, we refer to Slobbe (2013) and Farahani et al. (2017a).

To compute QG models I and III–V, we had to determine the depth of the basis functions of equations (5) and (7). By assessing the model error at a height anomaly control data set using one height anomaly control data set at a time, we found an optimal depth of 80 km. The second parameter to be determined is the effective regularization parameter λeff, based on which the two regularization parameters λ and λ' were computed (see equation (A6)). In doing so, we used Figure B1 that shows the a posteriori mean SD and the square root of the estimated variance factors as a function of the effective regularization parameter. The variance factors appear to be robust over a broad range (10^{-12}–10^{-9}) of regularization parameters. Among those regularization parameters, we used the smallest one (here, 10^{-12}), which represents a very weak regularization.

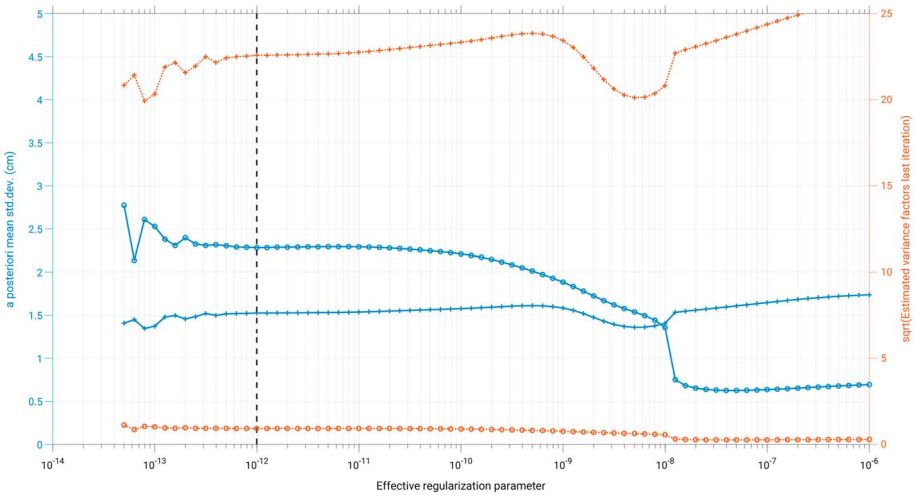

Figure B1. A posteriori mean standard deviations (solid lines) and square root of estimated variance factors (dotted lines) as a function of the effective regularization parameter for the global gravity model height anomaly data set (lines with the "o" markers) and the local height anomaly data set (lines with the "+" markers). These results are obtained using the computational setup of solution I.

Table B2 summarizes the results of the VCE applied in step 2 of the sequential parameter estimation procedure. Remember that the two data sets used in step 2 are low-pass filtered height anomaly data sets, that is, they represent spatial scales corresponding to spherical harmonic degrees not exceeding 230. For QG solution I, the estimated variance factor for the GGM height anomaly data set is 0.83; hence, the mean SD of this data set reduces from 2.5 to 2.28 cm. The estimated variance factor for the local height anomaly data set, however, is 509.93. Correspondingly, the mean SD for this data set increases from 0.068 to 1.52 cm. Hence, the contribution of the local height anomaly data set to the coarse scales of the QG model is significantly reduced after VCE has been applied compared to the contribution of the GGM height anomaly data set.

Currently, it is not possible to validate the result of the VCE, and we can only speculate whether the results are reasonable or not. Assuming that the noise VC matrices of both data sets are realistic (up to a scaling factor) and remembering that both data sets have the same size and share the same data points, the downweighting of the local height anomaly data set can only be explained by a more favorable covariance structure of the noise VC matrix of the GGM height anomaly data set compared to the one of the local height anomaly data sets. On the other hand, the noise VC matrix of the GGM height anomaly data set is highly ill conditioned (the condition number is about 10^{16}; see Klees et al., 2018). This, in combination with the necessary regularization when computing the least squares QG model, may have an impact on the results of the VCE. First experiments, which use Rao's pandora's box approach (Rao, 1971) in combination with a Kryolov subspace iterative solver, point to a downweighting of the local height anomaly data set relative to the GGM height anomaly data set of "only" a factor of 130. Computing a new QG solution I with the new variance factors improves the error statistics over the Netherlands to a level comparable to QG solution II, whereas

Table B2
Estimated Variance Factors and Posteriori SDs for the Two Height Anomaly Data Sets Used in Step 2 of the Sequential Parameter Estimation Procedure

QG solution	Data	No. of data points	Variance factor	A posteriori SD (cm)
I	GGM	126	0.83	2.28
	local	126	509.93	1.52
IV	GGM	126	0.81	2.32
	local	126	477.88	1.48
V	GGM	126	0.01	0.28
	local	126	5,919.50	5.19

Note. "GGM" refers to the GGM height anomaly data set and "local" refers to the local height anomaly data set. SD = standard deviation; QG = quasi-geoid; GGM = global gravity model.

the more favorable error statistics of QG solution I over Belgium do not change. This result, however, is preliminary, and further investigations are needed. However, it shows that the QG solution I is sensitive to the results of the VCE.

Appendix C: Control Data Sets

Two control data sets were available to validate the QG models.

GPS/leveling data over the Netherlands. The first data set comprises 84 points distributed over the Netherlands. Two of the 84 data points are reported as outliers by Crombaghs and de Bruijne (2004) and were not considered here. GPS measurements were acquired over the period 1996–1997 as part of the fifth precise leveling campaign (Brand et al., 2004). At each point, 5 days of GPS measurements were collected. For this study, we reprocessed all GPS measurements with the Bernese GPS Software Version 5.2 (Dach et al., 2015) using products from the second reprocessing campaign and station data of the International GNSS Service (IGS) (Dow et al., 2009). From this, reprocessed station coordinates were obtained in the IGb08 reference frame at the mean epoch of the GPS measurements, which is epoch 1997.9. As other data sets for this study refer to the International Terrestrial Reference Frame 2005 (ITRF2005; Altamimi et al., 2007), the station coordinates were transformed to ITRF2005 at epoch 1997.9 using the ITRF2008 to ITRF2005 transformation parameters (Altamimi et al., 2011). As a final preprocessing step, the GPS ellipsoidal heights were transformed from the tide free crust to the mean≡zero crust permanent tide system (Poutanen et al., 1996). The noise SD of the GPS ellipsoidal heights is about 5 mm.

The spirit leveling measurements were conducted within 1 month after the GPS data acquisition; therefore, potential vertical movements of the height markers do not affect the geometric height anomalies. The corrections associated with the adjustment of the first-order height network in 2005 have been applied (Brand et al., 2004). The NAP height system used in the Netherlands is a mean-tide system, that is, mean≡zero crust over mean geoid (Mäkinen & Ihde, 2008). As the QGs refer to the zero-tide system, we applied the corresponding transformation from mean-tide geoid to zero-tide geoid. The NAP heights were transformed to the EVRF2007 (in restoring the reference field, the geoid's potential value is set to the potential value for the EVRF2007 zero level surface) by adding 0.021 m. The formal error SDs of the NAP heights are shown in Figure C1. They range from 1.8 to 4.5 mm. The average SD is 3.1 mm. From this, we can estimate the SDs of the geometric height anomalies, which range from 5.3 to 6.7 mm, with a mean value of about 5.8 mm.

GPS/leveling data over Belgium. The second data set comprises 3,760 GPS height markers over Belgium. The GPS measurements were acquired during the period 2010–2017. Each point was observed in two sessions

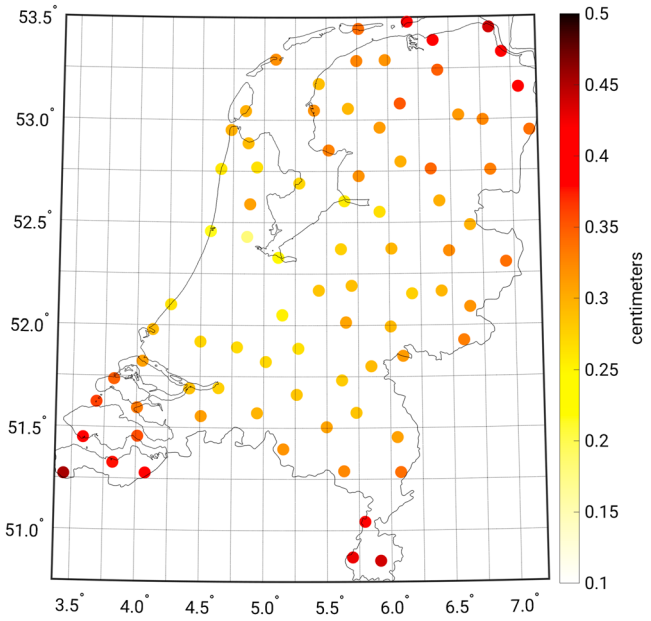

Figure C1. Formal errors of the NAP heights at the GPS/leveling stations over the Netherlands.

of three quarters of an hour. Ellipsoidal heights refer to the ITRF2005 at epoch 2012.167. No information about the noise SD of the GPS ellipsoidal heights is documented. Given the total record length of only 1.5 hr, we consider a noise SD of 10 mm as realistic.

Recently, the National Geographic Institute of Belgium performed a series of new least squares adjustments of the Belgian first-order height network (TAW). Here we used the results of an unconstrained adjustment in which only the height of one marker was fixed. The TAW height system is a mean-tide system. Also here, we applied the corresponding transformation from mean-tide geoid to zero-tide geoid. The TAW heights were transformed to the EVRF2007 by first transforming them to NAP (by adding −2.340 m) and then to EVRF2007 (by adding 0.021 m). The National Geographic Institute could not provide formal SDs for the newly adjusted TAW heights. However, the readjusted TAW heights differed by several centimeters from the official TAW heights. This may point to a SD above the value of 5 mm adopted for the NAP heights in the Netherlands. Considering a SD of 5 mm as a minimum value, the mean noise SD of the geometric height anomalies over Belgium is at least 11 mm.

Acknowledgments
This study was performed in the framework of the Netherlands Vertical Reference Frame (NEVREF) project, funded by the Netherlands Technology Foundation STW. This support is gratefully acknowledged. We thank the Editor and two anonymous reviewers for their constructive remarks and corrections, which helped us to improve the quality of the manuscript. The GOCO05s model can be obtained from their website (http://www.goco.eu/). Local high-resolution gravity data sets (terrestrial, shipboard, and airborne) were kindly provided by Rijkswaterstaat (available upon request), the University Utrecht, the Nationaal Geografisch Instituut (Belgium), the British Geological Service, the Nordic Geodetic Commission, Bundesamt für Kartographie und Geodäsie (Germany), Institut für Erdmessung (Germany), ExxonMobil (Germany), Engie (Germany), the Bureau Gravimétrique International (International Gravity Bureau) IAG service (France; http://bgi.obs-mip.fr/en), the Banque de données Gravimétriques de la France, and the Bureau de Recherches Géologiques et Minières (France). Radar altimeter data were obtained from the Radar Altimeter Database System (RADS) and are freely available through their website (http://rads.tudelft.nl/rads/rads.shtml). The Dutch GPS/leveling data were kindly provided by Kadaster/Rijkswaterstaat (available upon request). The Belgium GPS/leveling data were kindly provided by the Nationaal Geografisch Instituut.

References

Altamimi, Z., Collilieux, X., Legrand, J., Garayt, B., & Boucher, C. (2007). ITRF2005: A new release of the international terrestrial reference frame based on time series of station positions and earth orientation parameters. *Journal of Geophysical Research*, *112*, B09401. https://doi.org/10.1029/2007JB004949

Altamimi, Z., Collilieux, X., & Métivier, L. (2011). ITRF2008: An improved solution of the international terrestrial reference frame. *Journal of Geodesy*, *85*(8), 457–473. https://doi.org/10.1007/s00190-011-0444-4

Bachmaier, M., & Backes, M. (2011). Variogram or semivariogram? Variance or semivariance? Allan variance or introducing a new term? *Mathematical Geosciences*, *43*(6), 735–740. https://doi.org/10.1007/s11004-011-9348-3

Brand, G., van Brussel, G., ten Damme, J., & Gerritsen, J. (2004). Herberekening van het primaire net van het NAP - verbetering precisie en betrouwbaarheid ten behoeve van de nieuwe NAP publicatie (*AGI/GAP-04/004*). Delft: Adviesdienst Geo-informatie en ICT. (In Dutch).

Chambodut, A., Panet, I., Mandea, M., Diament, M., Holschneider, M., & Jamet, O. (2005). Wavelet frames: An alternative to spherical harmonic representation of potential fields. *Geophysical Journal International*, *163*(3), 875–899. https://doi.org/10.1111/j.1365-246X.2005.02754.x

Crombaghs, M., & de Bruijne, A. (2004). NLGEO2004 - Een nieuw geoïdemodel voor nederland (*AGI-GAP-2004-25*). Delft: Adviesdienst geo-informatie en ICT.

Dach, R., Lutz, S., Walser, P., & Fridez, P. (2015). *Bernese GNSS software version 5.2*. Bern: Astronomical Institute, University of Bern. https://doi.org/10.7892/boris.72297, User manual.

Denker, H. (2013). *Regional gravity field modeling: Theory and practical results* (pp. 185–291). Berlin Heidelberg, Berlin, Heidelberg: Springer. https://doi.org/10.1007/978-3-642-28000-9_5

Denker, H. (2015). *A new European gravimetric (quasi)geoid EGG2015*. Prague, Czech Republic: Poster presented at XXVI General Assembly of the International Union of Geodesy and Geophysics (IUGG), Earth and Environmental Sciences for Future Generations 22 June – 02 July 2015.

Ditmar, P., Klees, R., & Liu, X. (2007). Frequency-dependent data weighting in global gravity field modeling from satellite data contaminated by non-stationary noise. *Journal of Geodesy*, *81*(1), 81–96. https://doi.org/10.1007/s00190-006-0074-4

Dow, J. M., Neilan, R. E., & Rizos, C. (2009). The international GNSS service in a changing landscape of global navigation satellite systems. *Journal of Geodesy*, *83*(3), 191–198. https://doi.org/10.1007/s00190-008-0300-3

Farahani, H. H., Slobbe, D. C., Klees, R., & Seitz, K. (2017a). Impact of accounting for coloured noise in radar altimetry data on a regional quasi-geoid model. *Journal of Geodesy*, *91*(1), 97–112. https://doi.org/10.1007/s00190-016-0941-6

Farr, T. G., Rosen, P. A., Caro, E., Crippen, R., Duren, R., Hensley, S., et al. (2007). The shuttle radar topography mission. *Reviews of Geophysics*, *45*, RG2004. https://doi.org/10.1029/2005RG000183

Forsberg, R. (1984). A study of terrain reductions, density anomalies and geophysical inversion methods in gravity field modelling (*5*). Columbus, Ohio, USA: Ohio state univ columbus dept of geodetic science and surveying.

González, Á. (2010). Measurement of areas on a sphere using fibonacci and latitude-longitude lattices. *Mathematical Geosciences*, *42*(1), 49–64. https://doi.org/10.1007/s11004-009-9257-x

Grafarend, E. W., & Schaffrin, B. (1993). *Ausgleichungsrechnung in Linearen Modellen*. Mannheim: BI-Wissenschaftsverlag.

Heck, B., & Seitz, K. (2007). A comparison of the tesseroid, prism and point-mass approaches for mass reductions in gravity field modelling. *Journal of Geodesy*, *81*(2), 121–136. https://doi.org/10.1007/s00190-006-0094-0

Hirt, C., & Seeber, G. (2008). Accuracy analysis of vertical deflection data observed with the Hannover Digital Zenith Camera System TZK2-d. *Journal of Geodesy*, *82*(6), 347–356. https://doi.org/10.1007/s00190-007-0184-7

Holschneider, M., & Iglewska-Nowak, I. (2007). Poisson wavelets on the sphere. *Journal of Fourier Analysis and Applications*, *13*(4), 405–419. https://doi.org/10.1007/s00041-006-6909-9

Hovenbitzer, M. (2008). The European DEM (EuroDEM)—Setup and harmonisation, *The international archives of the photogrammetry* (Vol. 37, pp. 1853–1856), Remote Sensing and Spatial Information Sciences. Beijing, China: ISPRS Congress.

Klees, R., & Slobbe, D. (2018). Impact of systematic errors in gravity and heights on a quasi-geoid model for the Netherlands and Belgium, contribution to the commemorative publication for Bernhard Heck.

Klees, R., Slobbe, D., & Farahani, H. (2017). A methodology for least-squares local quasi-geoid modelling using a noisy satellite-only gravity field model. *Journal of Geodesy*, *92*, 431–442. https://doi.org/10.1007/s00190-017-1076-0

Klees, R., Slobbe, D., & Farahani, H. (2018). How to deal with the high condition number of the noise covariance matrix of gravity field functionals synthesised from a satellite-only global gravity field model? *Journal of Geodesy*, *93*, 29–44. https://doi.org/10.1007/s00190-018-1136-0

Koch, K.-R., & Kusche, J. (2002). Regularization of geopotential determination from satellite data by variance components. *Journal of Geodesy*, *76*(5), 259–268. https://doi.org/10.1007/s00190-002-0245-x

Kusche, J. (2003). A Monte-Carlo technique for weight estimation in satellite geodesy. *Journal of Geodesy*, *76*, 641–652. https://doi.org/10.1007/s00190-002-0302-5

Lieb, V., Bouman, J., Dettmering, D., Fuchs, M., & Schmidt, M. (2016). Combination of GOCE gravity gradients in regional gravity field modelling using radial basis functions. In N. Sneeuw, P. Novák, M. Crespi, & F. Sansò (Eds.), *VIII Hotine-Marussi symposium on mathematical geodesy* (pp. 101–108). Cham: Springer International Publishing.

Mäkinen, J., & Ihde, J. (2008). The permanent tide in height systems. In F. Sansò & M. G. Sideris (Eds.), *Observing our changing Earth* (Vol. 133, pp. 81–87), International Association of Geodesy Symposia. Berlin Heidelberg: Springer.

Mayer-Gürr, T., Kvas, A., Klinger, B., Rieser, D., & Zehentner, N. (2015). *The new combined satellite only model GOCO05s*. Vienna, Austria: EGU General Assembly 2015. https://doi.org/10.13140/RG.2.1.4688.6807

Olesen, A. V., Andersen, O. B., & Tscherning, C. C. (2002). Merging of airborne gravity and gravity derived from satellite altimetry: Test cases along the coast of Greenland. *Studia Geophysica et Geodaetica*, *46*, 387–394. https://doi.org/10.1023/A:1019577232253

Pail, R., Goiginger, H., Schuh, W.-D., Höck, E., Brockmann, J. M., Fecher, T., et al. (2010). Combined satellite gravity field model GOCO01S derived from GOCE and GRACE. *Geophysical Research Letters*, *37*, l20314. https://doi.org/10.1029/2010GL044906

Poutanen, M., Vermeer, M., & Mäkinen, J. (1996). The permanent tide in GPS positioning. *Journal of Geodesy*, *70*, 499–504. https://doi.org/10.1007/BF00863622

Rao, C. (1971). Estimation of variance and covariance components—MINQUE theory. *Journal of Multivariate Analysis*, *1*(3), 257–275. https://doi.org/10.1016/0047-259X(71)90001-7

Rao, C. (1971). Unified theory of linear estimation. *Sankhyā: The Indian Journal of Statistics, Series A*, *33*, 371–394. corrigendum (1972), 34, p. 194 and p. 477.

Reuter, R. (1982). Über Integralformeln der Einheitssphäre und harmonische Splinefunktionen. Veröff. Geod. Inst. RWTH Aachen, 33.

Sandwell, D. T., & Smith, W. H. F. (1997). Marine gravity anomaly from GEOSAT and ERS 1 satellite altimetry. *Journal of Geophysical Research*, *102*, 10,039–10,054. https://doi.org/10.1029/96JB03223

Schuh, W.-D., Müller, S., & Brockmann, J. M. (2015). Completion of band-limited data sets on the sphere. In H. Kutterer, F. Seitz, H. Alkhatib, & M. Schmidt (Eds.), *The 1st International Workshop on the Quality of Geodetic Observation and Monitoring Systems (QuGOMS'11)* (pp. 171–178). Cham: Springer International Publishing.

Sjöberg, L. E. (2005a). A discussion on the approximations made in the practical implementation of the remove-compute-restore technique in regional geoid modelling. *Journal of Geodesy*, *78*(11–12), 645–653. https://doi.org/10.1007/s00190-004-0430-1

Sjöberg, L. E. (2011). Local least squares spectral fitting and combination by harmonic functions on the sphere. *Journal of Geodetic Science*, *1*, 355–360. https://doi.org/10.2478/v10156-011-0015-x

Slobbe, D. C. (2013). Roadmap to a mutually consistent set of offshore vertical reference frames (Ph.D. thesis), Delft University of Technology.

Slobbe, D. C., Verlaan, M., Klees, R., & Gerritsen, H. (2013a). Obtaining instantaneous water levels relative to a geoid with a 2d storm surge model. *Continental Shelf Research*, *52*, 172–189. https://doi.org/10.1016/j.csr.2012.10.002

Smith, W. H. F. (2010). The marine geoid and satellite altimetry (1st ed.). In V. Barale, J. F. R. Gower, & L. Alberotanza (Eds.), *Oceanography from space revisited* (pp. 181–193). New York: Springer.

Tachikawa, T., Hato, M., Kaku, M., & Iwasaki, A. (2011). Characteristics of ASTER GDEM version 2. In *2011 IEEE International Geoscience and Remote Sensing Symposium* (pp. 3657–3660). Vancouver, BC, Canada. https://doi.org/10.1109/IGARSS.2011.6050017

Tenzer, R., & Klees, R. (2008). The choice of the spherical radial basis functions in local gravity field modeling. *Studia Geophysica et Geodaetica*, *52*(3), 287–304. https://doi.org/10.1007/s11200-008-0022-2

Tikhonov, A. (1963). Solution of incorrectly formulated problems and the regularization method. *Soviet Mathematics Doklady*, *4*, 1035–1038.

Wenzel, H. G. (1982). Geoid computation by least squares spectral combination using integral formulas. In *Proceedings of general meeting of the IAG*, Tokyo, pp. 438–453. 7-15 May, 1982.

Wittwer, T. F. (2009). Regional gravity field modelling with radial basis functions. Delft: Delft University of Technology, Nederlandse Commissie voor Geodesie Publikatie 72.

Wu, Y., Zhou, H., Zhong, B., & Luo, Z. (2017). Regional gravity field recovery using the GOCE gravity gradient tensor and heterogeneous gravimetry and altimetry data. *Journal of Geophysical Research: Solid Earth*, *122*, 6928–6952. https://doi.org/10.1002/2017JB014196

Zijl, F., Verlaan, M., & Gerritsen, H. (2013). Improved water-level forecasting for the northwest european shelf and north sea through direct modelling of tide, surge and non-linear interaction. *Ocean Dynamics*, *63*(7), 823–847. https://doi.org/10.1007/s10236-013-0624-2